Effects of fuel cetane number on the structure of diesel spray combustion: an accelerated Eulerian stochastic fields method

M. Jangi[*,a], T. Lucchini[b], C. Gong[a], X.-S. Bai[a]

[a] *Div. Fluid Mechanics, Dept. of Energy Sciences, Lund University, 22100 Lund, Sweden*

[b] *Politecnico di Milano, Dipartimento di Energetica, Milano, Italy*

Abstract

Eulerian stochastic fields (ESF) method accelerated with chemistry coordinate mapping (CCM) approach for modeling spray combustion is formulated, and applied to model of diesel combustion in constant volume vessel configuration. In ESF-CCM, the thermodynamic states of the discretized stochastic fields is mapped into a low dimensional phase space. Integration of the chemical stiff ODEs is performed in the phase space and the results are mapped back into the physical domain. Using ESF-CCM, effects of fuel cetane number on the structure of diesel spray combustion is investigated. It is shown that depending of the fuel cetane number, liftoff length is varied and the combustion mode is changed. Spray combustion with a shorter liftoff length exhibits characteristics of the classical conceptual diesel combustion model proposed by Dec (SAE paper 970873, 1997) whereas in a case with a lower cetane number the liftoff length is much larger and, the spray combustion is likely occurred in a lean-premixed mode of combustion.

Keywords:
transported PDF, acceleration technique, diesel spray flames

[*]corresponding author
Email address: mehdi.jangi@energy.lth.se (M. Jangi[*,a])

1. Introduction

Predictive modeling of diesel spray combustion is a unique and powerful tool to better understand and cop with engine-out emissions behavior in direct injection (DI) internal combustion (IC) engine applications. Among several key parameters, the liftoff length (distance from the nearest reacting site to the injector nozzle) is of great importance. It is known that larger liftoff length can provide longer time for mixing between the evaporated injected fuel and the ambient oxidizer. Enhancing mixing prior to the ignition onset is in favor of reducing engine-out particulate matter emissions.

Four different mechanisms for the stabilization of lifted flames and prediction of liftoff length have been proposed in the literature. These mechanisms are: (1) fuel and oxidizer are premixed within the liftoff height such that the base of a lifted flame burns as a turbulent premixed-flame [1], which implies that a lifted flame is stabilized where the turbulent flame speed is balanced by the incoming reactant velocity [2]; (2) fuel and oxidizer remain non-premixed within the liftoff height such that the base of a lifted-flame burns as a diffusion-flame [3], which implies that a lifted-flame is stabilized at the location where the local scalar dissipation rate is equal to the critical dissipation rate at extinction; and (3) fuel and oxidizer are partially premixed within the liftoff height such that a lifted-flame at its base burns as an edge-flame [4] which is made up of a lean premixed branch, a rich premixed branch and a diffusion flame (the so-called triple-flame) that intersect at the triple-point. The main difference between propagation of an edge-flame and that of a stoichiometric premixed-flame is that the incoming reactant stream diverges significantly due to the heat release from the edge-flame; therefore, the effective flame-front-normal component of the incoming velocity at the base of an edge-flame is smaller than that of the main stream velocity further upstream in the flow [5]. Together with curvature effects, this leads to a propagation speed that is significantly larger than the propagation speed of an unstrained stoichiometric premixed-flame [4–6]; (4) The primarily stabilization mechanism of lifted jet flame discharging into a high temperature environment is autoignition in fuel-lean side of the jet [7–10]. In this way liftoff position is at the location where the convection rate of reactants stream is balanced by the chemical rate of reactions. In the other words liftoff length is determined by the ignition delay time of the most ignitable sites.

In our previous study on a partially premixed lifted jet flame discharging into a high temperature environment, we showed that depending on the

liftoff position, combustion modes can vary from a triple flame structure with obvious lean-premixed, rich-premixed and diffusion-flame branches to lean-premixed flame [10]. Among many evidences provided by others [7–9, 11], results of that study implied that a successful predictive modeling of spray combustion in advanced IC engine like conditions that employ multiple injection and exhaust gas recirculation should potentially be able to cop with lean-rich premixed and diffusion flames as well as auto-ignition mode of combustions. Transported probability density function (PDF) method is shown to be capable of handling universal modes of combustion [12, 13]. This is due to the fact that in the PDF formulation of a turbulent reacting system, the chemical source terms are appeared in a closed form, hence, no further assumptions need to be made on the structure and mode of combustion to take to account the so called "chemistry-turbulence interaction". The PDF method has been proposed in two major formulations: the Lagrangian based [12] and the Eulerian based [14] approach, known as Eulerian stochastic fields method. Regardless of the approach that is adopted, the integration of chemical stiff ODEs is usually the most time consuming part of the modeling procedure.

In general, any measure that accelerates the integration of the chemistry ODEs proportionally reduces the overall computational cost. Chemical mechanism reduction and chemistry tabulation/storage/retrieval approach [15] are common examples of such techniques. *In situ* adaptive tabulation (ISAT) [16] is an example of tabulation/storage/retrieval approach. While ISAT can significantly reduce the computational costs in statistically stationary flows, it is less efficient in non-stationary flows. Transient spray combustion and combustion in internal combustion (IC) engines are examples of applications where the advantage of ISAT have proven elusive.

To address this issue, a key aspect of the approach proposed here is the employment of the newly developed chemistry coordinate mapping (CCM) technique [10, 17–19] to accelerate the transported PDF method. This approach was initially formulated and validated using a Lagrangian based PDF method [10]. Here we extend the method by coupling the CCM approach to the Eulerian based PDF method.

2. Mathematical model: The stochastic fields method accelerated with CCM

In this study spray is modeled using Eulerian-Lagrangian method. The gas phase is described in Eulerian frame with the unsteady Reynolds-averaged Navier Stock (URANS) equations. The liquid phase is presumed to be a discrete phase consisting of individual parcels and treated in Lagrangien particle tracting (LPT) fashion. Each parcel represents a range of spherical droplets, and the parcels are tracked in the Lagrangian framework. Gas and liquid phases are coupled through the mass, momentum, chemical reactions and energy exchange source terms between the phases. OpenFOAM [20] is used for numerical solution of the governing equations. Implicit second order schemes are used for both temporal and spatial terms. Transport properties of each species are evaluated using NASA's seven polynomial coefficients. Further details on the governing equations and spray sub-model can be found in our previous publications [21, 22].

The PDF method that is used here employs an Eulerian stochastic fields method [14]. In the ESF method, turbulent reactive flows are represented by N_F stochastic fields. The stochastic equation for n^{th} stochastic field is:

$$\begin{aligned}\overline{\rho}d\phi_\alpha^{(n)} &= -\overline{\rho}\tilde{u}_i\tfrac{\partial\phi_\alpha^{(n)}}{\partial x_i}dt + \overline{\rho}S_\alpha^r(\boldsymbol{\phi^{(n)}})dt + \overline{\rho}S_\alpha^s(\boldsymbol{\phi^{(n)}})dt \\ &+\tfrac{\partial}{\partial x_i}(\Gamma_t\tfrac{\partial\phi_\alpha^{(n)}}{\partial x_i})dt - \tfrac{1}{2}\overline{\rho}C_\phi(\phi_\alpha^{(n)} - \tilde{\phi}_\alpha)\omega_t dt + \overline{\rho}\sqrt{2\tfrac{\Gamma_t}{\overline{\rho}}}\tfrac{\partial\phi_\alpha^{(n)}}{\partial x_i}d\boldsymbol{W_i}^{(n)}\,,\end{aligned} \tag{1}$$

The above equation imply invoking the gradient transport hypothesis for approximating transport by turbulent velocity fluctuations. Here $\Gamma_t = \frac{\mu}{\sigma} + \frac{\mu_t}{\sigma_t}$ is the total molecular plus turbulent diffusivity, mu_t is turbulent viscosity, σ_t is turbulent Schmidt or Prandtl number as it appearers in transport equitations of chemical species or conservation of energy. $S_\alpha^r(\boldsymbol{\phi}^{(n)})dt$ is increments in $\phi_\alpha^{(n)}$ due to chemical reactions and $S_\alpha^s(\boldsymbol{\phi}^{(n)})dt$ is increments in $\phi_\alpha^{(n)}$ due to spray.

The term involves C_ϕ is the molecular mixing which is modeled by Interaction with Exchange to the Mean (IEM) model and ω_t in this term is the turbulent frequency obtained from $\omega_t = \epsilon/k$ with k and ϵ being the turbulent kinetic energy dissipation rate.

The $d\boldsymbol{W_i}^{(n)}$ represents a vector Wiener process that is spatially uniform but different for each field. Here $d\boldsymbol{W_i}^{(n)}$ is approximated by time-step increment $\sqrt{dt}\eta^{(n)}$ and $\eta^{(n)}$ is a $\{-1, 1\}$ dichotomic random vector [14].

The mean and moments of each variable α can be approximated from the ensemble of N_F stochastic fields, for example the mean is:

$$\tilde{\phi}_\alpha = \frac{1}{N_F} \sum_{n=1}^{N_F} \phi_\alpha^{(n)} \tag{2}$$

An operator splitting strategy is used to isolate the chemical source terms. The calculation of those source terms involves evaluating the integral $\int_{t_0}^{t_0+dt} S_\alpha(\boldsymbol{\phi}^{(n)})dt$. A potentially more efficient way to evaluate the chemical source terms would be to first identify and cluster all cells in all stochastic fields that have similar thermodynamic states into phase-space zones, and then perform the ODE integration once for all of the particles in the zone. This approach is known as clustering [23], or sometimes is referred to as an agglomeration [24] technique.

The CCM approach as proposed in [17, 18] is adopted for clustering. In principle, the CCM phase space consists of a subset of the composition space. The mapping of the n^{th} field with composition $\boldsymbol{\phi}^{(n)}(Y_1, ..., Y_{N_S}, h)$ into the discretized phase space can be considered as a mapping between the CFD cell index (i, j, k) in n^{th} to the zone index in discretized phase space. The (i, j, k) CFD cell at time t in n^{th} field is mapped to the l^{th} zone in direction α of the phase space according to

$$\begin{aligned} &q_\alpha^{(n)}(i, j, k, t) = l, \\ &\quad if \;\; \zeta_\alpha(l) \leq \phi_\alpha^{(n)}(i, j, k, t) < \zeta_\alpha(l) + \Delta\zeta_\alpha \;\; (\alpha = 1, 2, ..., N_S + 1), \end{aligned} \tag{3}$$

where $\Delta\zeta_\alpha$ is the mesh size in the discretized phase space. Here, $\zeta_\alpha(l)$ is the coordinate of the phase space,

$$\zeta_\alpha(l) = \zeta_\alpha^{min}(t_n) + (l - 1)\Delta\zeta_\alpha, \tag{4}$$

where $\zeta_\alpha^{min}(t_n)$ is the minimum value ϕ_α over all notional fields at time t_n.

Each zone in the phase space corresponds typically to multiple cells in the notional fields. An integer zone index, Z_{id}, is assigned to each notional field such that each zone index denotes one point in the discretized phase space,

$$Z_{id}^{(n)}(i, j, k, t) = \sum_{\alpha=1}^{N_S+1} \prod_{r=1}^{\alpha-1} N_r q_\alpha^{(n)}(i, j, k, t), \tag{5}$$

where N_r is the total number of zones in ζ_r and $\prod$ is the product symbol. This zone index facilitates to store mapping cells into a one dimensional

array rather than a multi-dimensional Cartesian phase space. In this way the memory requirements for the CCM will massively reduced, because memory is only allocated to the zones that contains at least one cell of the notional fields, hereinafter the "active zone".

The mass-averaged value of ϕ_α in the active zones of the phase space (denoted by $\hat{\phi}_\alpha$) is calculated following the mapping:

$$\begin{aligned}\hat{\phi}_\alpha(\eta_1, \eta_2, ..., \eta_{N_S+1}, t) &= \hat{\phi}_\alpha(Z_n, t) \\ &= \frac{1}{m_{Z_n}} \sum_{n=1}^{N_{Z_n}} \{m^{(n)}(i,j,k,t)\phi_\alpha^{(n)}(i,j,k,t) | Z_{id}^{(n)}(i,j,k,t) = Z_n\},\end{aligned} \tag{6}$$

where $m_{Z_n} = \sum_{n=1}^{N_{Z_n}} \{m^{(n)}(i,j,k,t) | Z_{id}^{(n)}(i,j,k,t) = Z_n\}$ is the total mass in the Z_n^{th} zone of the phase-space, and N_{Z_n} is the total number of cells mapped into the Z_n^{th} phase-space zone. The mass-averaged $\hat{\boldsymbol{\phi}}(Z_n, t_n)$ is the composition vector that is used during the chemistry integration operation step, and the results after the integration are assigned to all cells in the $Z^{(n)}$ zone. Errors due to mapping and mass averaging can be minimize by refining the phase space resolution.

Equations (3-6) can be used for any number of species. However, not all species are equally important in the determination of the particle's thermodynamic state. Reduced descriptions of turbulent reactive flows (e.g., [25] and references therein) are frequently used where the composition vector $\boldsymbol{\phi}_\alpha^{(n)}(Y_1, ..., Y_{N_S}, h)$ may be described by a reduced number of independent variables $\phi_\alpha^{(n)}(Y_1, ..., Y_{N_R}, h)$ and $N_R < N_S$. Jangi et al. [17, 18, 21] in DNS and RANS studies of premixed and partially premixed combustion of hydrogen, methane, syngas (a blend of CO and H_2) and n-heptane have shown that computational cells at a given time can be mapped into a phase space $(T, J_H, \nabla J_H \cdot \nabla J_H, Y_{fuel})$. Here, J_H is the mass fraction of hydrogen atom, and $\nabla J_H \cdot \nabla J_H$ is analogous to the scalar dissipation rate. The same strategy is adopted here; instead of mapping to $\phi_\alpha^{(n)}(Y_1, ..., Y_{N_S}, h)$ or $\phi_\alpha^{(n)}(Y_1, ..., Y_{N_R}, h)$, a mapping is carried out into (T, ξ, χ, Y_{fuel}) space, where ξ is mixture fraction and χ is scalar dissipation rate. The sensitivity of the results to various extensions of the phase-space dimensionality, e.g., mapping to higher-dimensional $(T, \xi, \chi, Y_1, Y_2, ..., Y_{N_R})$ can be found in our previous works [10, 17, 18, 21].

In this study we use Bilger's mixture fraction ξ [26] as one dimension in the phase space, whereas in our previous work, mass fraction of hydrogen element, J_H, was used [17]. Using J_H is preferable when preferential diffusion is taken into account [17], which is not the case here. Bilger's mixture fraction for the n^{th} field, $\xi^{(n)}$, is

$$\xi^{(n)} = \frac{0.5(J_H^{(n)} - J_{H,o}) + 2(J_C^{(n)} - J_{C,o}) - (J_O^{(n)} - J_{O,o})}{0.5(J_{H,f} - J_{H,o}) + 2(J_{C,f} - J_{C,o}) - (J_{O,f} - J_{O,o})}, \tag{7}$$

where J_H, J_C and J_O are element mass fractions and subscripts "o" and "f" indicate the oxidizer and fuel streams, respectively.

$$\chi^{(n)} = 2(\overline{D} + \frac{\mu_t}{Sc_t})\nabla\xi^{(n)} \cdot \nabla\xi^{(n)}, \tag{8}$$

It is known that scalar dissipation rate is usually exponentially decaying along the downstream direction in the mixing region of a free jet. Therefore, discretizing the phase space in the χ coordinate with uniform $\Delta\chi$ is not efficient; $exp(-\chi)$ is used as the phase-space variable, instead. This is equivalent to disceretizing phase space in the χ coordinate with a nonuniform grid. For all other variables, a uniform grid is employed.

3. Results and discussion

The baseline case that is presented here correspond to the Engine Combustion Network (ECN) constant volume vessel "spray H" (n-heptane spray) combustion at 21% Oxygen level, ambient temperature of 1000 K and ambient density of 14.8 [Kg/m^3] [27]. This case is served for model validations. In addition to the baseline case, two cases with different fuel cetane number are also adopted. Different cetane number is obtained by varying the ratio of isc-octane with a cetane number of 15 to n-heptane with a cetane number of 56 in the liquid fuel composition. Table 1 lists the details of each case setup. In this study we use a kinetic mechanism that has been developed for self-ignition of mixtures of iso-octane and n-heptane known as primary reference fuel (PRF) [28]. The mechanism involves 18 species and 19 reactions. PRF is usually used as a surrogate fuel in research projects to replicate different octane/cetane number of practical fuels. The number appears after "PRF" shows the volumetric concentration of iso-octane in the fuel mixture. In Table 1, PRF0, PRF50 and PRF100 correspond to fuels with 0% (pure n-heptane), 50% and 100% iso-octane, respectively. In this way, case PRF0

Table 1: List of cases and their setup; for all cases ambient is at: oxygen level of 21%, temperature of 1000 [K] and density of 14.8 [Kg/m^3].

case	C7H16 %	C8H18 %	cetane no.
PRF0	100	0	56
PRF50	50	50	35.5
PRF100	0	100	15

represents the ECN spray-H baseline case while cases PRF50 and PRF100 are designed to investigate the effects of fuel cetane number on the structure of spray combustion.

A 2D-axisymmetric domain was used in which grids were refined toward the spray axis in radial direction and were uniform in direction of the spray axis. The total number of grids points is approximately 12000. This grids is based on our previous work in the same configuration [29]. In this study, we used 50 numbers of stochastic fields. Further increasing of the number of fields dose not improve the simulation results. In our previous work, we showed that when CCM method is used to accelerate a Lagrangian based PDF method, a CCM phase space consisting of (ξ, T, χ, Y_{fuel}) is required and enough to uniquely map all notional particles into the CCM phase space [10]. Here the same CCM phase space with $(\xi, T, \chi, Y_{C7H16}, Y_{C8H18})$ dimensions is adopted. Note that for case PRF0 only Y_{C7H16} and for case PRF100 only Y_{C8H18} presents, therefore, the corresponding CCM phase space for these cases is reduced to a four dimensional space.

It is known that χ is usually exponentially decaying along the downstream direction in the mixing region of a free jet. Therefore, discretizing the CCM phase space in the χ coordinate with uniform $\Delta\chi$ is not efficient; $exp(-\chi)$ is used as the phase-space variable, instead. This is equivalent to disceretizing phase space in the χ coordinate with a nonuniform grid. For all other variables, a uniform grid is employed. As for the CCM phase space resolution we use for all cases $\Delta\xi$=0.01, ΔT= 5 K, $\Delta exp(-\chi)$=0.025 and $\Delta Y_{C_7H_{16}}$=$\Delta Y_{C_8H_{18}}$=0.01. This resolution is based on our previous study where Lagrangian based PDF method was coupled with CCM method to simulated a partially premixed lifted flame [10].

Figure 1 shows the vessel pressure rise history. Ignition delay time in the baseline case, PRF0, has been slightly over-predicted. This is partly due to the kinetic mechanism that is used in this study. Nevertheless, the trend of

the process has been properly reproduced by the model, especially, the sloop of the curve after auto-ignition delay time and during the linear part of the chart agrees well with the experimental data. More important is that the method employed here could successfully predict the cetane number effect on the ignition delay time. As it is evident in the figure, when the PRF number of fuel is increased (larger iso-octane content in the fuel mixture) the ignition delay time is increased.

Liftoff length is another parameter that can be used for model validation. The experimental measurement of the liftoff length is 17 mm from the nozzle. This length was based on an OH chemiluminescence imaging. Fig. 2 shows a snapshot of temperature and the root mean square (RMS) of temperature fluctuations after 1.5 ms from start of injection. At this time liftoff position was fairly steady in the experiment as it was so in the simulation. OH chemiluminescence does not exist in the kinetic mechanism that is used here, instead, we use an iso-contour of temperature at 1200 K to identify the reacting region and the liftoff position. It can be seen in Fig. 2 that the liftoff position has been predicted, properly. Structure of combustion in this condition also agrees well with the conceptual diesel combustion model proposed by Dec [30] (shown in the right hand side in Fig. 2).

According to the Dec's conceptual model, in a diesel combustion, injected fuel is evaporated and mixed with the ambient oxidizer and form a rich-premixed mixture of reactants. This fuel rich mixture reactants are burnt in a form of a rich-premixed burnt flame at the liftoff position. Combustion products of the rich-premixed burnt flame are mainly unburnt hydrocarbons, carbon monoxide, hydrogen which will further oxidized by the ambient oxidizer at the periphery diffusion-flame. Different region and modes of combustion have been shown schematically in the right hand side in Fig. 2, after Dec. We will comeback to the conceptual model in the following sections.

Figure 3 shows the predicted liftoff length as a function of PRF number. Recalling zero in x-axis corresponds to case PRF0, 50 to PRF50 and 100 to PRF100, as the PRF number increases the liftoff length is increased. It can be seen that liftoff length for PRF100 is more than three times larger than that of PRF0. This is a consequence of smaller cetane number (longer ignition delay time) in case PRF100. Previously, we showed that depending on the ambient temperature, the structure of lifted partially premixed jet flame discharging into a high temperature environment can changed from a triple-flame with obvious lean-rich premixed and diffusion flames to an only lean-stoichiometric premixed flame [10]. Here, we examine the effects

of liftoff length on the structure of spray combustion.

Shown in Figs. 4 and 4 are snapshots of temperature and the RMS of temperature fluctuations at a typical time during the quasi-steady period of combustion (approximately 1 after start of ignition). To identify the high temperature region of the domain, iso-contour of temperature at 1200 K is also shown by a solid white line in these plots. It can be seen that temperature distribution in cases PRF0 and PRF50 are rather similar and temperature in these cases is higher than that of case PRF100. Temperature fluctuations for PRF0 and PRF50 near the liftoff position is maximized whereas for PRF100 at the liftoff position the fluctuations are rather smaller. Fig. 6 shows the distribution of oxygen mass fraction, Y_{O2}. It can be seen that after liftoff position, and inside the high temperature region for cases PRF0 and PRF50, no oxygen molecule has left. This feature mimics the conceptual diesel spray combustion proposed by Dec [30] that discussed earlier and shown in Fig. 2. However, in case PRF100, oxygen is still left in high temperature region of the domain. Presence of oxygen after liftoff position in the high temperature region can be due to an incomplete fuel-rich premixed combustion or a fuel-lean premixed combustion.

The difference between combustion mode in these cases is better seen in the scattered plot of temperature-equivalence ratio as it shown in Fig. 7. This scattered plot corresponds to the entire domain. In this plot, black circles symbol correspond to case PRF0, red rectangles to case PRF50 and green diamonds to case PRF100. The highest temperature in PRF100 is lower than that of cases PRF0 and PRF50, which consistent with the previous figure. More important is that in case PRF100, all points in the high temperature region of the plots, e.g., temperature above 1200 K, have an equivalence ratio less than unity, indicating a fuel-lean premixed combustion in case PRF100. However, the high temperature region of cases PRF0 and PRF50 covers from fuel-rich to stoichiometry to fuel-lean mixtures. Nevertheless, by decreasing the fuel cetane number from case PRF0 to PRF50, the fuel rich region in the high temperature region of the plot suppressed. This is a consequence of a larger liftoff length in case PRF50 that provides a better premixing prior to the onset of auto-ignition.

Figures Fig. 4-7 imply that cases PRF0 and PRF50 are burning as a classical diesel combustion with a rich-premixed burnt flame right after the liftoff position whereas case PRF100 is a fuel-lean premixed combustion. A better illustration of the different combustion modes can be given by flame index [31]. Flame index is usually used to identify premixed and non-premixed

flames. The normalized flame index [32], FI, may be defined as

$$FI = \frac{1}{2}(1 + \frac{\nabla Y_{Fu} \cdot \nabla Y_{Ox}}{|\nabla Y_{Fu} \cdot \nabla Y_{Ox}|}). \tag{9}$$

Here subscript Fu and Ox refer to fuel and oxidizer components. Within the high temperature reacting region, FI approaches to zero when combustion is in diffusion-flame mode while it approaches to unity when combustion is in premixed-flame mode.

Flame index for different cases are shown in Fig. 8. In case PRF0, at the liftoff position three branches can be seen. The lean-premixed burnt branch that is located in the oxidizer side, the rich-premixed branch that is located in the vicinity of the spray axis, and the diffusion-flame branch that is sandwiched in between of the two. These three branches meet at the liftoff position and form a triple flame structure. Very similar structure is seen in case PRF50 with the an slightly weaker indication of the diffusion-flame branch at the triple point. In case PRF100; however, the structure is very different. Here there is no triple flame structure and combustion in the high temperature region of the domain has a non-zero flame index, indicating a premixed burnt combustion. This is consistent with the snapshot of oxygen distribution. This result confirms that spray combustion in case PRF100 is of a lean premixed combustion. Flame temperature of a lean-premixed burnt gases is lower than a diffusion-flame that is burnt at the stoichiometry. This explain the lower temperature of combustion products in case PRF100 compared with that in cases PRF0 and PRF50 as can be seen in Fig. 4.

In our previous work, we showed that the primary stabilization mechanism of methane/air lifted partially premixed jet flames discharging into the high temperature environment is auto-ignition processes [10] while the liftoff length and thereby the structure of combustion is largely changed as the ambient temperature is changed. Here also, although the liftoff length and structure of combustion are largely changed as the fuel cetane number is changed, identifying the stabilization mechanism at the liftoff position required a further examination. Transport budges at at the liftoff position can be revealing. Fig. 9 shows the rate of reactions and diffusion at the liftoff position as a function of progress variable c. Reaction rates and progress variable in this figure is calculated based on CO_2 species. It is evident that the reaction rate in all cases is larger that the diffusion rate by several orders of magnitude. This is a typical characteristic of auto-ignition process in which reaction rate is balanced by the convection rate whereas, in a flamelet-like

of combustion reaction rate is balanced by diffusion rate. This behavior is consistent with our previous observation in the case of methane/air lifted jet flame [10] and imply that for all cases studied here the primary stabilization mechanism is auto-ignition process regardless of the mode of combustion in the downstream flow after the liftoff location.

4. Conclusions

Numerical simulations of diesel spray combustion with URANS formulation was performed. Eulerian stochastic fields method was used as a combustion sub-model. The method was accelerated with chemistry coordinate mapping (CCM) technique. Results showed that the method is capable of handling combustion modes from lean-rich premixed to diffusion-flame modes.

It was shown that depending on the fuel cetane number different mode of combustion can occur. At high cetane number where ignition delay time is shorter, e.g., case PRF0, the liftoff length is smaller and spray combustion exhibits a pattern of the conceptual diesel spray model proposal by Dec [30]. At lower cetane numbers; however, e.g., PRF100, the ignition delay time and the liftoff length are both increased. A larger liftoff length can provide enough time for premixing prior to the liftoff position. The combustion mode under this condition is very different from the classical diesel combustion. Results showed that when liftoff length is large enough, no triple flame at the liftoff position and diffusion-flame at the periphery of the reacting region is formed. Spray combustion in this condition exhibits a lean-premixed combustion mode characteristics. Nevertheless, analysis of the transport budget at the liftoff position revealed reaction rates is larger by several order of magnitude than the rate of diffusion which is typical characteristic of the auto-ignition and imply that the primary stabilization mechanism for all cases with various cetane number is auto-ignition process.

Acknowledgments: This work was sponsored by the Swedish Research Council (VR). The computation was performed using Lindgren cluster at PDC center for high performance computing center and the Swedish National Infrastructures for Computing (SNIC).

References

[1] L. Vanquickenborne, A. van Tiggelen, Combust. Flame 10 (1966) 59–69.

[2] H. Eickhoff, B. Lenze, W. Leuckel, Proc. Combust. Inst. 20 (1985) 311–318.

[3] N. Peters, F. Williams, AIAA J. 21 (1983) 423–429.

[4] J. Buckmaster, R. Weber, Proc. Combust. Inst. 26 (1996) 1143–1148.

[5] J. Buckmaster, R. Weber, Combust. Flame 134 (2003) 355–368.

[6] G. Ruetsch, L. Vervisch, A. Linan, Phys. Fluids 7 (1995) 1447–1454.

[7] R. Cabra, J.-Y. Chen, R. Dibble, A. Karpetis, R. Barlow, Combust. Flame 143 (2005) 491–506.

[8] R. L. Gordon, A. R. Masri, S. B. Pope, G. M. Goldin, Combust. flame 151 (2007) 495–511.

[9] C. S. Yoo, R. Sankaran, J. H. Chen, J. Fluid Mech. 640 (2009) 453–481.

[10] M. Jangi, X. Zhao, D. Haworth, X.-S. Bai, Combut. flame (2014) DOI: 10.1016/j.combustflame.2014.07.031.

[11] K. Gkagkas, R. Lindstedt, Proc. Combust. Inst. 31 (2007) 1559–1566.

[12] S. B. Pope, Prog. Energ. Combust. Sci. 11 (1985) 119–192.

[13] D. C. Haworth, Prog. Energ. Combust. Sci. 36 (2010) 168–259.

[14] L. Valino, Flow, Turbulence and Combustion 60 (1998) 157–172.

[15] T. Echekki, E. Mastorakos, Springer (2011).

[16] L. Lu, S. B. Pope, J. Computa. Phys. 228 (2009) 361386.

[17] M.Jangi, R. Yu, X. Bai, Combust. Theory Modeling 16 (2012) 221–249.

[18] M.Jangi, X. Bai, Combust. Theory Modeling 16 (2012) 1109–1132.

[19] M.Jangi, R. Yu, X. Bai, Flow, Turbulence and Combustion 16 (2012) 1109–1132.

[20] The open source CFD toolbox available at http://www.openfoam.com (????).

[21] M. Jangi, T. Lucchini, G. D'Errico, X. Bai, Proc. Combust. Inst. 34 (2013) 3091–3098.

[22] C. Gong, M. Jangi, T. Lucchini, G. D'Errico, X.-S. Bai, Flow turbulence and combustion (2014) DOI 10.1007/s10494–014–9566–0.

[23] L. Liang, J. G. Stevens, J. T. Farrell, Combust. Sci. Technology 181 (2009) 13451371.

[24] G. M. Goldin, Z. Ren, S. Zahirovic, Combust. Theory Modeling 4 (2009) 721–739.

[25] Z. Ren, G. M. Goldin, V. Hireman, S. Pope, Combust. Theory Modeling 6 (2011) 827–848.

[26] R. W. Bilger, S. H. Starner, R. J. Kee, Combust. Flame 80 (1990) 135–149.

[27] (????).

[28] S. Voglsam, F. Winter, Chem. Eng. J. 203 (2012) 357369.

[29] K. M. Pang, M. Jangi, X.-S. Bai, J. Schramm, SAE paper 2014-01-1254 (2014).

[30] J. Dec, SAE paper 970873 (1997).

[31] Y. Mizobuchi, J. Shinjo, S. Ogawa, T. Takeno, Proc. Combust. Inst. 30 (2005) 611–619.

[32] B. Fiorina, O. Gicquel, L.Vervisch, S. C. N. Darabiha, Combust. flame 140 (2005) 147–190.

List of Figures

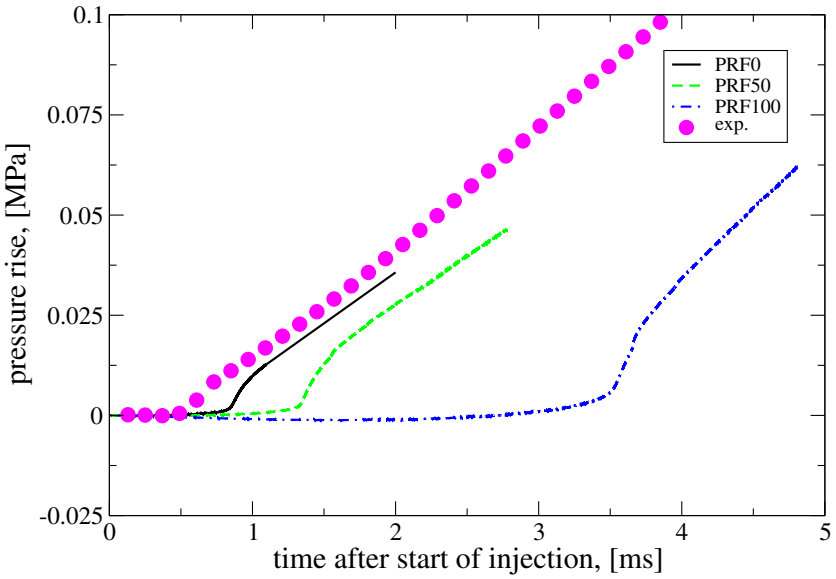

Figure 1: Pressure rise for various PRF numbers.

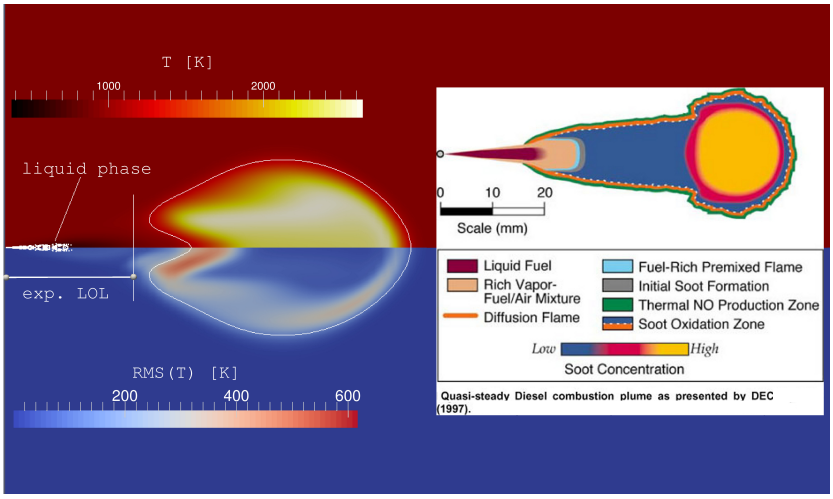

Figure 2: Snapshot of temperature and its RMS after 1.5 ms from start of injection for baseline case; vertical solid line shows the liftoff position measured in the experiment.

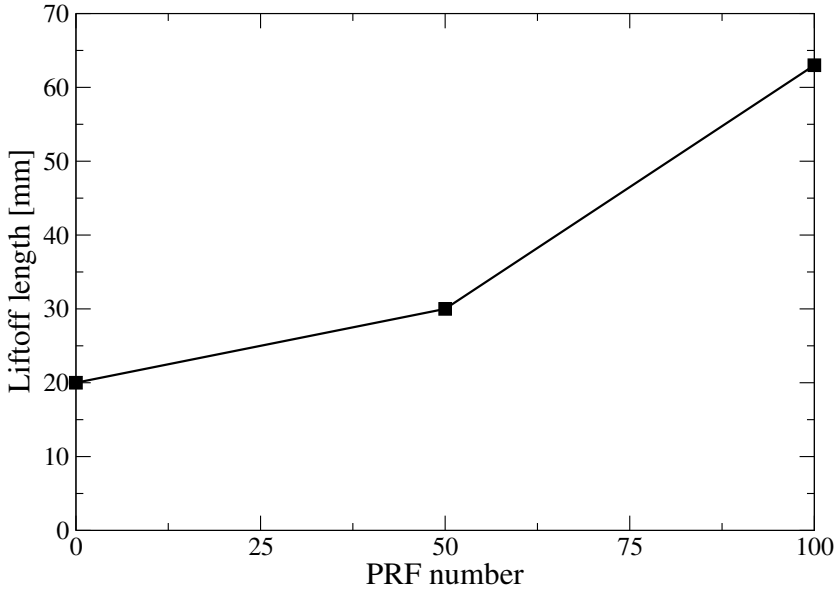

Figure 3: Predicted liftoff length during quasi steady period of spray combustion at various PRF numbers.

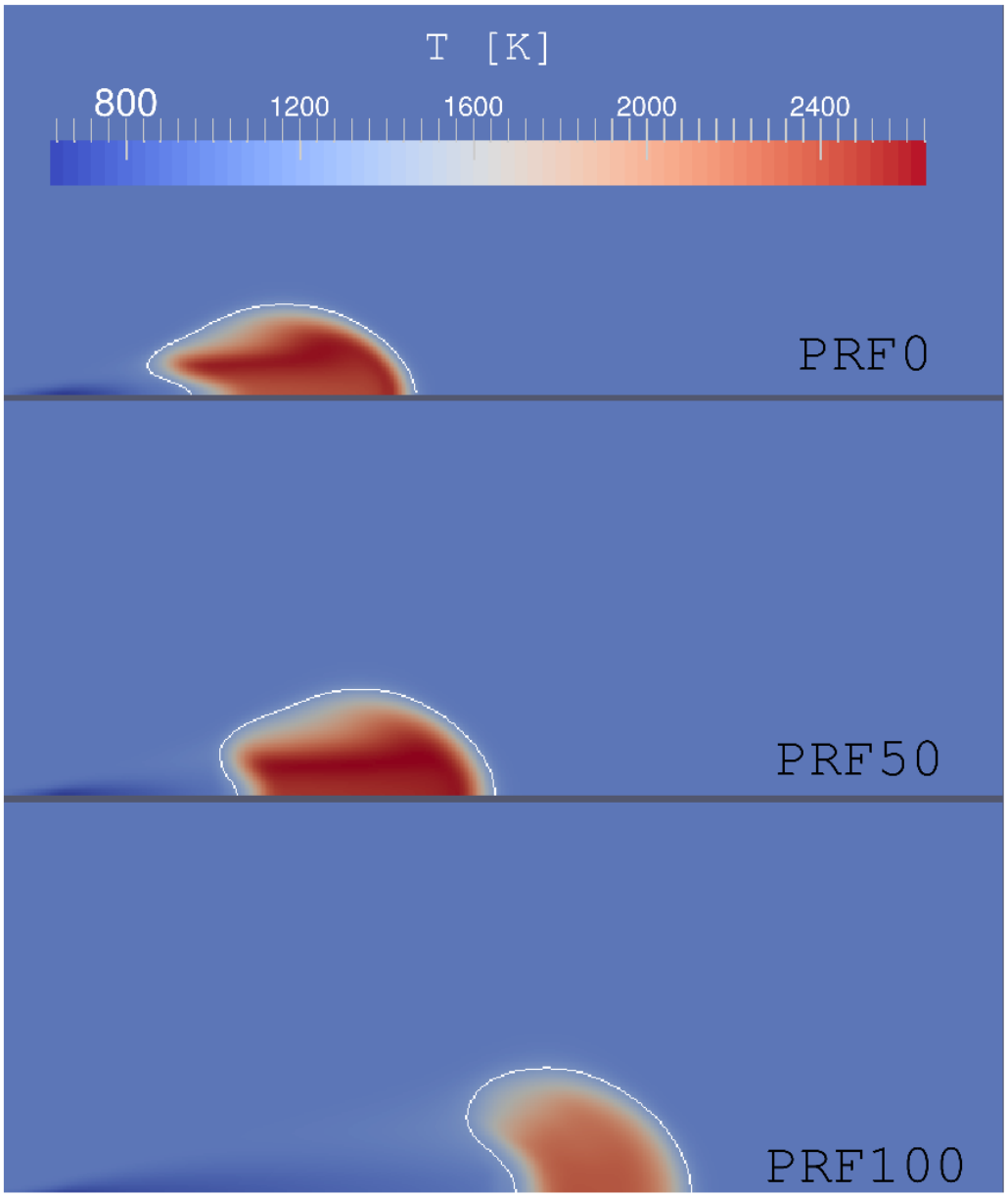

Figure 4: Temperature at a typical time during quasi-steady state of combustion (approximately 1 ms after the start of ignition). High temperature region of domain has been identified by the iso-contour temperature at 1200 K shown by a solid white color line in the figures.

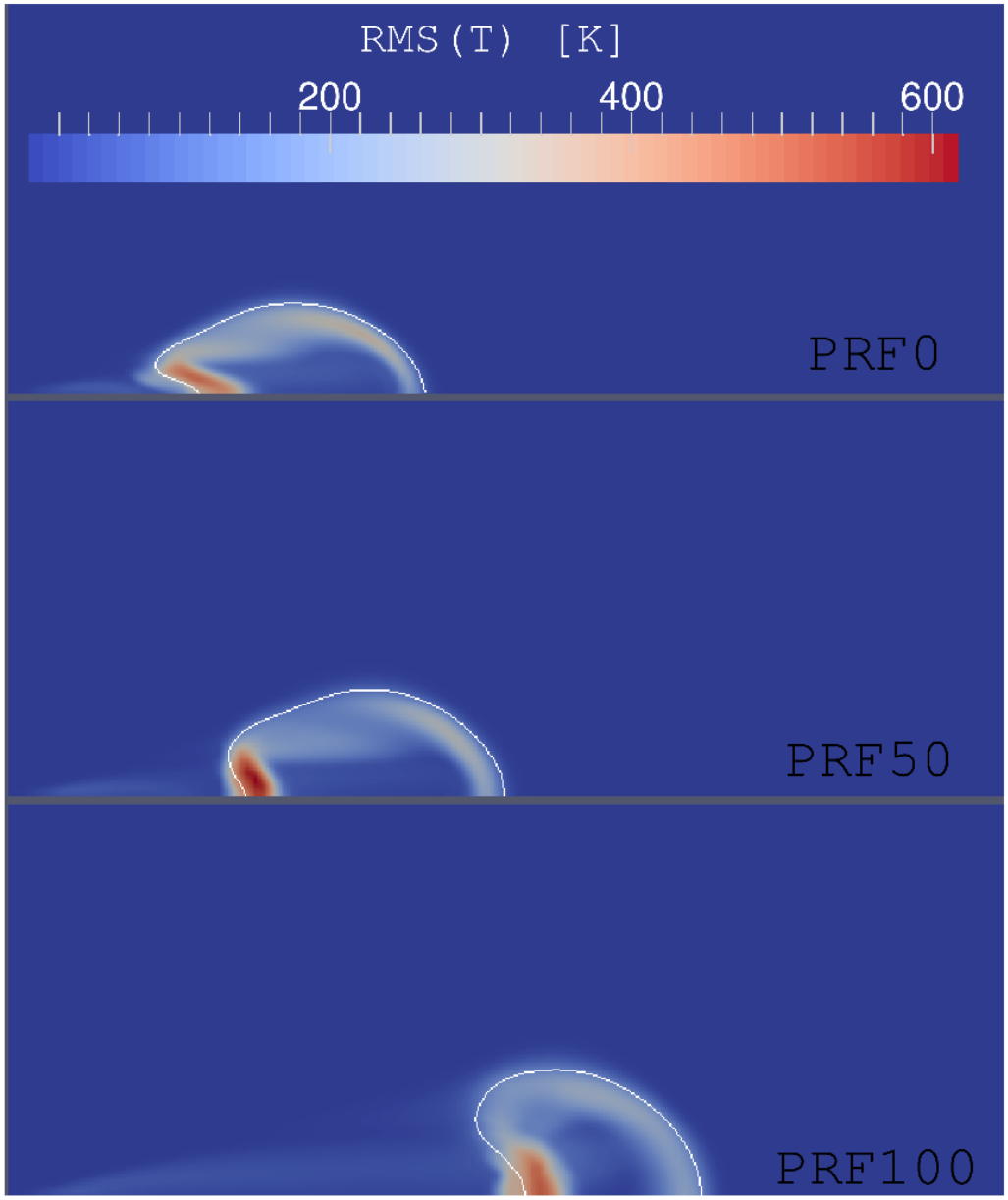

Figure 5: RMS fluctuations at a typical time during quasi-steady state of combustion. Contours as in the caption of Fig. 4.

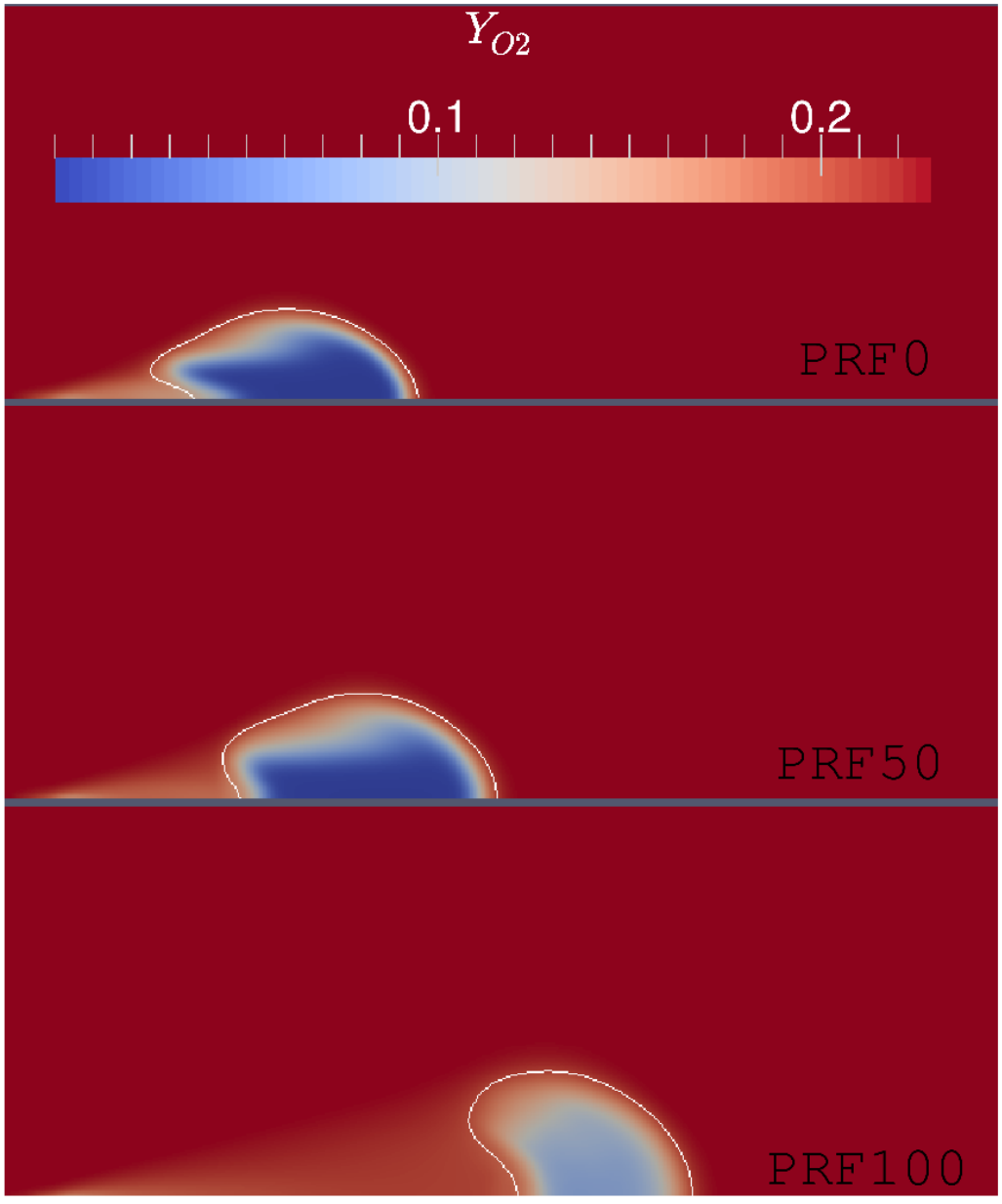

Figure 6: Oxygen mass fraction, Y_{O2}, at a typical time during quasi-steady state of combustion. Contours as in the caption of Fig. 4.

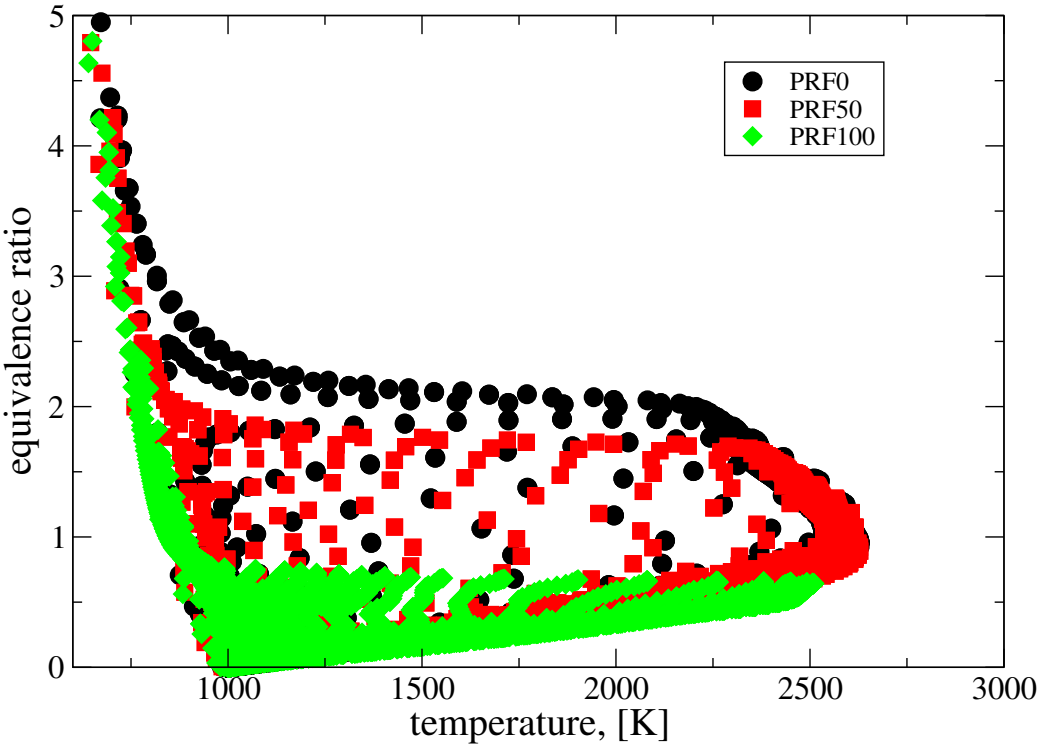

Figure 7: scattered-plot of temperature-equivalence ratio for cases PRF0, PRF50 and PRF100 at a typical time during quasi-steady state of combustion. Contours as in the caption of Fig. 4

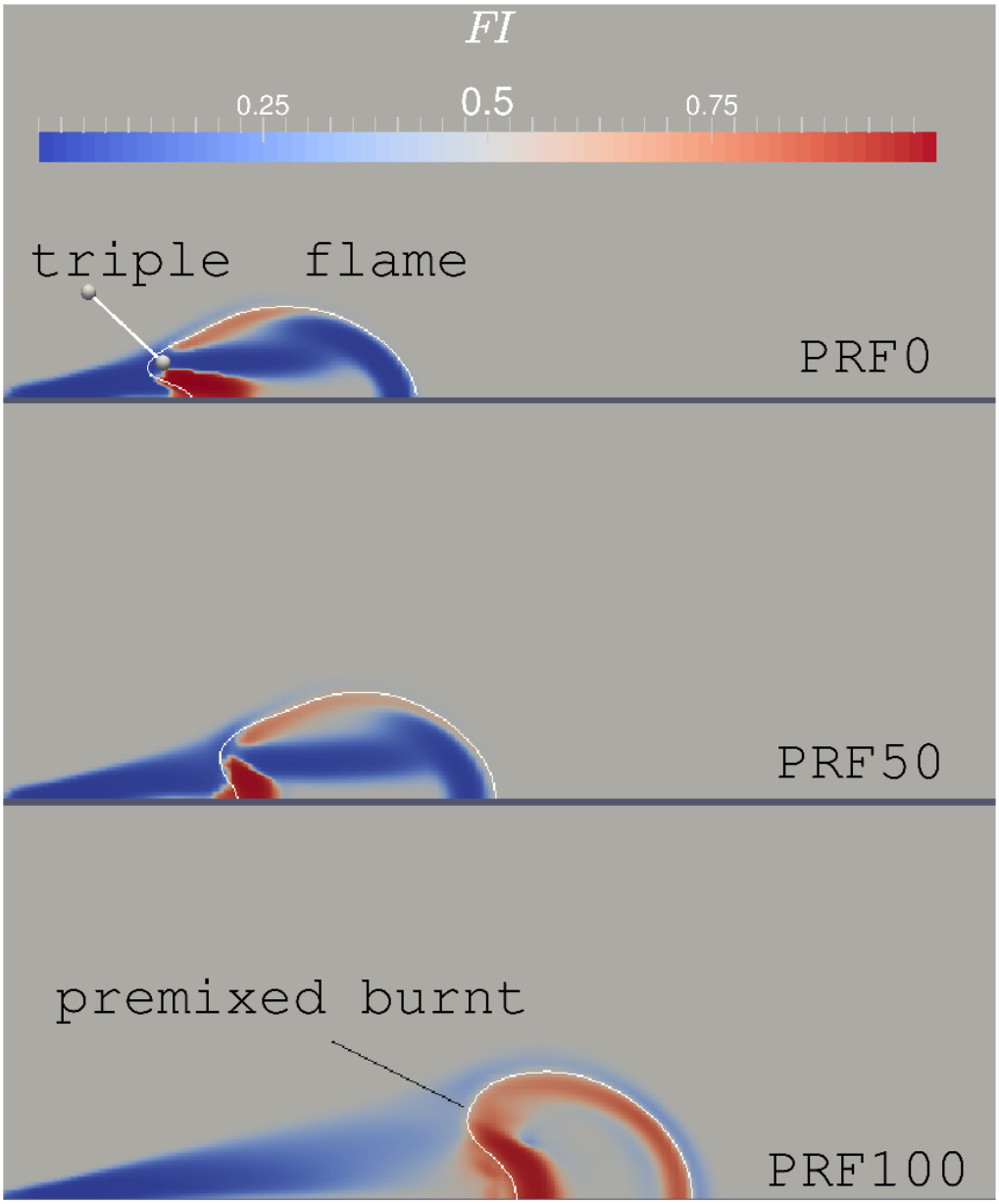

Figure 8: Normalized flame index, FI at a typical time during quasi-steady state of combustion. Diffusion flame is identified by FI=0 and premixed flame by a non-zero flame index. Contours as in the caption of Fig. 4.

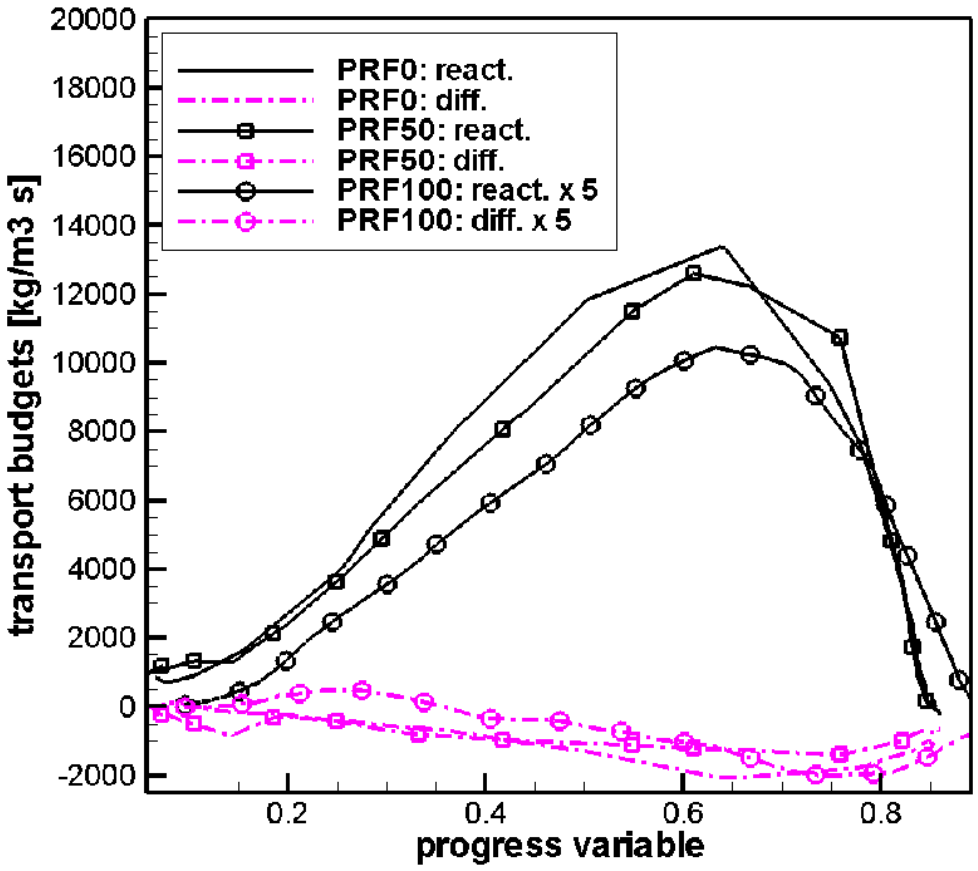

Figure 9: Transport budget at the liftoff position at a typical time during quasi-steady state of combustion.